Aug 15, 2003

Phase-Referenced VLBA Observations of OH Masers at 4765 MHz

Patrick Palmer

Department of Astronomy and Astrophysics, University of Chicago, 5640 S. Ellis Ave., Chicago, IL 60637

ppalmer@oskar.uchicago.edu

W. M. Goss

National Radio Astronomy Observatory, Socorro, NM 87801

mgoss@nrao.edu

and

K. E. Devine[1]

Carleton College, Northfield, MN 55057

devinek@carleton.edu

ABSTRACT

We report VLBA observations of maser emission from the rotationally excited $^2\Pi_{1/2}, J = 1/2$ state of OH at 4765 MHz. We made phase-referenced observations of W3(OH) at both 4765 MHz and 1720 MHz and found emission in three fields within a ∼2000 AU diameter region and verified that in two of the three fields, 4765 MHz and 1720 MHz emission arise from the same position to within ∼4 mas (∼8 AU). We imaged DR21EX without phase-referencing and detected six ∼5 AU diameter emission regions along an approximately N-S arc with linear extent ∼500 AU. In addition, we carried out phase-referenced observations of 4765 MHz emission from K3-50. We searched for the 4765 MHz line in W49 (without phase referencing) and W75N (phase-referenced to the strongest 4765 MHz maser feature in DR21EX); we were unable to detect these sources with the VLBA. For 2 1/2 years (including the dates of the VLBA observations), we carried out monitoring observations of 4765 MHz emission with the VLA. Constraints on models for maser emission at 1720 MHz and 4765 MHz are derived from the observations. These observations are then briefly compared with existing models.

Subject headings: ISM: individual(DR21EX, K3-50, W3(OH))—masers—radio lines: ISM—techniques: interferometric

1. Introduction

OH masers have long been associated with the early stages of star formation. Models of maser pumping mechanisms allow constraints to be set on the physical conditions in the region of the maser. By understanding the conditions associated with OH masers, the conditions in regions of star formation can be delineated. Many models have been developed for pumping mechanisms for the ground state (18 cm wavelength) lines; a number of the models have been extended to excited state masers. One of these excited states is the $^2\Pi_{1/2}, J = 1/2$. The most commonly detected line from this state is the satellite F=1 $\rightarrow$ 0 transition at 4765 MHz. Although there are several models for emission from this state (e.g. Kylafis & Norman 1990; Cesaroni & Walmsley 1991; Gray et al. 1992; and Pavlakis & Kylafis 1996a,b), these models are not entirely satisfactory. Detailed observations are required including higher spatial resolution and absolute position determinations.

Previous studies with increasing accuracies have shown many instances of spatial coincidence between 1720 MHz ground state masers and 4765 MHz masers (Cesaroni & Walmsley 1991; Masheder et al. 1994; Gray et al. 2001 (hereafter GCRYF)). The possible spatial overlap has been an important factor in recent pumping models. In particular, the study of GCRYF with MERLIN provided the first absolute positions of 4765 MHz and 1720 MHz masers in W3(OH). To within the uncertainties (estimated to be 5 mas at 4765 MHz and 15 mas at 1720 MHz), they found that in two of three fields the positions of the two masers agreed. In addition, they compared angular sizes of 1720 MHz masers (Masheder et al. 1994) to those of accompanying 4765 MHz masers and found that the 4765 MHz masers are considerably larger, implying a smaller gain at the higher frequency.

Another important feature of 4765 MHz masers is their polarization properties. Theoretically, if polarization of molecular emission lines arises from magnetic effects, these lines should be unpolarized because the Landé g-factor of this state is $\sim$0 (Dousmanis et al. 1955). Probably because because polarization is not expected, little observational effort has been expended to measure polarization of these lines. To date polarization has been detected in only one source. During a spectacular flare, the 4765 MHz maser in MonR2 was found to be 15% linearly polarized (Smits et al. 1998). Amplification of an unseen polarized background source was a suggested cause. Recently, Dodson & Ellingsen (2002) obtained upper limits for polarization in a survey of southern star-forming regions. The most stringent limits for the 16 sources in which 4765 MHz emission was detected were $\leq$4% linear and $\leq$5% circular.

Spatial coincidence with maser emission in other OH transitions, angular size measurements, and polarization all provide information about possible pumping mechanisms in these masers. Furthermore, existing models for 4765 MHz emission focus largely on W3(OH). By observing a number of other sources, we are able to examine whether these models are more generally applicable.

In this paper we report VLBA observations of 4765 MHz masers in W3(OH), DR21EX, and

[1]current address: University of Wisconsin, Department of Astronomy, 475 N. Charter Street, Madison, WI 53706

K3-50 as well as negative results for W49 and W75N. We also provide a preliminary report of VLBA observations of 1720 MHz emission in W3(OH).

Depending on the availability of a nearby reference source, the VLBA observations were made using phase-referencing. Phase-referencing serves two important purposes in this study: first, this technique provides a good initial phase correction so that narrow, relatively weak maser lines (peak flux densities $\leq$1 Jy) can be imaged with the VLBA; second, this technique permits absolute position determinations. This experiment improves previous investigations for the following reasons: 1) the synthesized beam of the VLBA is about an order of magnitude smaller that the MERLIN beam, 2) we measured all four Stokes parameters for 4765 MHz masers, and 3) we observed additional sources.

2. VLBA Observations and Analysis

All 4765 MHz observations were carried out using the National Radio Astronomy Observatory[2] (NRAO) Very Long Baseline Array (VLBA) in 2000 December 23 (W3(OH)) and 2001 February 19 and 24 (K3-50, DR21EX, W75N, and W49). Observations of the latter sources were interleaved over the two days to optimize hour angle coverage. Phase-referencing on nearby calibrators was used for W3(OH) and K3-50: scans of 3 minutes duration were made on a target source followed by 2 minute duration observations of the nearby reference source (see Table 1). Because of the current paucity of calibrators near the Galactic plane, phase-referencing could not be used for W49, W75N, and DR21EX. However, because DR21EX has some very strong features, these could be used as the phase-reference calibrator to determine phase corrections for W75N (although, of course not for the absolute position). For DR21EX and W75N, 3 minute scans were made on each. Ten antennas were used in all observations: either all VLBA antennas or (in December) one antenna from the Very Large Array (VLA) was substituted for the Pie Town antenna. Data was taken in 128 spectral channels spaced by 3.91 kHz in all four polarization combinations. With uniform weighting of the spectrum, this resulted in a velocity resolution of 0.29 km s^{-1} across $\sim$32 km s^{-1} from which all four Stokes parameters could be imaged. When phase-referencing was used, the accuracy of the absolute positions reported here is dominated by residual effects which were not removed by phase-referencing. This error is estimated to be $\pm$1 mas at 6 cm. This error is dominant when comparing our results to those of others or our results at 4765 MHz to those at 1720 MHz. The relative errors for positions at the same frequency in the same source are determined by thermal noise and are $\sim$0.1 mas for all reported measurements.

The 1720 MHz observations of W3(OH) were carried out with the VLBA on 2002 July 31. All 10 antennas of the VLBA were used. Phase-referencing was used with the same cycle as used for

[2]The National Radio Astronomy Observatory is a facility of the National Science Foundation operated under cooperative agreement by Associated Universities, Inc.

the 4765 MHz observations W3(OH). Data was taken in 1024 spectral channels spaced by 0.488 kHz. With uniform weighting, this resulted in a velocity resolution of 0.085 km s^{-1} across ∼80 km s^{-1}. Because these lines were previously known to be strongly circularly polarized, only right and left circular were observed. As at 4765 MHz, the accuracy of the absolute positions determinations is dominated by residual ionospheric effects which were not removed by phase-referencing. This error is estimated to be ±5 mas at 1720 MHz. For all reported results, the relative position errors determined by thermal noise are ∼0.1 mas.

Pointing positions were obtained from VLA measurements, and therefore are accurate at the 1″ level (Gardner et al. 1983; Palmer et al. 2003). The pointing positions[3], calibrators, distances to the reference sources, and total times on source are provided in Table 1.

[3]Most VLA positions quoted in this paper and the positions input for the VLBA observations are in the B1950 system. This convention was for compatibility with earlier measurements. In this paper, positions obtained from VLBA observations will be given in the J2000 system, and we will use this system for future measurements.

Table 1: Pointing Positions and Calibrators

Source	α_{1950}	δ_{1950}	Phase-Reference Source	Distance (degree)	Bandpass Calibrator	Total (minute)
W3(OH)						
4765 MHz:	02 23 16.45	61 38 57.51	0223+671	5.5	DA193	540
1720 MHz:	02 23 16.40	61 38 57.30	0223+671	5.5	3C454.3	460
K3-50	19 59 50.172	33 24 21.42	J2025+3343	4.9	3C454.3	104
DR21EX	20 37 13.552	42 14 01.23	—	—	3C454.3	106
W75N	20 36 50.11	42 26 58.49	DR21EX	0.2	3C454.3	101
W49	19 07 47.319	09 00 20.53	—	—	3C454.3	90

The data reduction was performed using standard AIPS software, following the guidelines set out in Appendix C of the AIPS Cookbook. This appendix contains instructions for spectral line phase-referenced imaging. During the final calibration steps, SETJY and CVEL were added to the steps outlined in the Cookbook before the data were split and imaged. Self calibration was used to improve the signal to noise ratio of the images; the rms noise level obtained was about 5 mJy per beam. During reduction, data from the Saint Croix and Mauna Kea antennas were deleted because the sources were resolved on these long baselines. Images were then made of all the spectral channels using the AIPS task IMAGR. At 4765 MHz, images were made for all four Stokes parameters; at 1720 MHz, images were made separately for left and right circular polarization. The synthesized beam was typically 3 – 4 mas at 4765 MHz and ∼6 mas at 1720 MHz for the resulting images. Detailed results for each source are provided in Section 4.

3. VLA Monitoring Observations

During the course of the experiment and shortly afterward, the sources observed with the VLBA at 4765 MHz were monitored with the VLA. Monitoring was important so that any significant time variability could be identified, and so that the flux densities observed with the VLBA could be compared with those observed with the VLA to determine the fraction of flux density resolved out with the VLBA.

The observations are summarized in Table 2. Both different configurations of the VLA and different spectrometer setups were used, resulting in varying spatial (third column) and spectral (fifth column) resolutions. In all cases, the VLA data were Hanning smoothed. The line emission was unresolved spatially, except for the A-array observations of W3(OH) on 2002 January 11 and April 22. In these observations, three closely spaced point sources are obvious which correspond to the three fields studied in more detail with the VLBA (Section 4.1). Because of the varying spectral resolution, we integrated the flux density in each spectrum and computed velocity centroids; thus, we could compare quantities that do not depend on spectral resolution. The observed velocity-integrated fluxes and the velocity centroids for W3(OH), DR21EX, and K3-50 are provided in Table 3. Although there may be variability at the 10 – 20 percent level, there is no evidence for episodes of large variability in the 2 1/2 years of observations of W3(OH), DR21EX, and K3-50 reported in this paper.

Table 2. VLA Array and Spectrometer setup for 4765 MHz Observations

Date	Array	Beam ($''$)	n_{chan}	ΔV (km s^{-1})	V_{total} (km s^{-1})	Source list
2000 Jan 30	B	2x1	127	0.384	47	DR21EX
2001 Mar 02	B	3x1	127	0.768	94	DR21EX, W75N, W3(OH), W3(C)
2001 Jun 12	B	7x2	127	0.384	47	DR21EX, W3(OH), W3(C)
2001 Aug 10	C	4x4	127	0.384	47	W49N, K3-50
2001 Aug 26	C	5x4	63	0.192	11	W3(OH)
2001 Aug 27	C	9x4	63	0.192	11	DR21EX
2001 Nov 15	D	14x12	63	0.192	11	DR21EX, K3-50, W3(OH), W3(C)
2002 Jan 11	D-A	0.4x0.3	127	0.096	11	W3(OH), W3(C)
2002 Apr 22	A	0.4x0.3	127	0.096	11	W3(OH)
2002 Jun 01	BnA	2x0.5	127	0.768	94	W49N
2002 Jul 24	B	1x1	63	0.192	11	DR21EX, K3-50

On 2001 August 10, we observed two features in W49 with the VLA. The peak flux densities were 162 mJy at V_{LSR}= 11.89 km s^{-1} and 437 mJy at V_{LSR}=2.28 km^{-1}. Without a phase-reference source, a flux density $\geq$ 1 – 2 Jy/beam is necessary to calibrate in the narrow frequency channels used for the VLBA observations. Because there was no phase-reference source available for W49, detection of the signals measured on 2001 August 10 with the VLA would have been impossible with the VLBA.

We also searched for W75N which had been observed to be highly variable in the last 20 years (summarized by Palmer et al. 2003). On 2001 March 02, the peak flux density was only 33 mJy; it is not surprising that we were unable to detect it with the VLBA after phase-referencing to DR21EX.

As a possible future VLBA target, we also searched for emission from the W3 continuum source (W3(C)). Highly variable emission from this position has been observed from time to time over the years (Gardner et al. 1983; Smits 1997). On 2001 June 12, we detected a 9-σ signal (flux density: 58 mJy/beam) in a single 0.348 km s^{-1} spectral channel at $\alpha(B1950)$ = 02 21 53.29±0.06, $\delta(B1950)$ = 61 52 23.4±0.3, V_{LSR}=-37.6 km s^{-1} . On 2001 March 02, we had detected a 5-σ signal with flux density about 50% of the value on 2001 June 12 in a single 0.768 km s^{-1} spectral channel at the same position and velocity. These results are consistent with non time-variable emission because of the differing spectral resolution.

Table 3: 4765 MHz Fluxes and Velocity Centroids from VLA and VLBA Observations

Date	W3(OH)		DR21EX		K3-50	
	Flux (Jy*km s^{-1})	Velocity (km s^{-1})	Flux (Jy*km s^{-1})	Velocity (km s^{-1})	Flux (Jy*km s^{-1})	Velocity (km s^{-1})
2000 Jan 30	—	—	2.4	4.23	—	—
2000 Dec 23	1.1	-43.94	—	—	—	—
2001 Feb 19/24	—	—	1.5	3.97	0.86	-20.35
2001 Mar 02	3.2	-44.41	2.7	4.00	—	—
2001 Jun 12	3.4	-44.41	2.6	3.99	—	—
2001 Aug 10	—	—	—	—	0.84	-20.26
2001 Aug 26	3.4	-44.31	—	—	—	—
2001 Aug 27	—	—	2.6	3.88	—	—
2001 Nov 15	3.9	-44.26	3.0	3.85	1.1	-20.25
2002 Jan 11	3.8	-44.26	—	—	—	—
2002 Apr 22	3.5	-44.31	—	—	—	—
2002 Jul 24	—	—	2.7	3.69	0.83	-20.23

4. VLBA Observational Results

The 4765 MHz VLBA observations of W3(OH), K3-50, and DR21EX were imaged in all four Stokes parameters. W49 and W75N proved too weak to detect with the VLBA. The results from imaging are discussed in this section. Only preliminary results for the 1720 MHz observations in W3(OH) will be presented here.

4.1. W3(OH)

4.1.1. 4765 MHz Observations

We found three regions of maser activity in the field of view. The relative positions of the three fields (referred to as fields 1, 2 and 3) are displayed in Figure 1, which shows the emission observed with the VLA A-array on 2002 April 22. The best estimate for the distance to W3(OH) is 2 kpc (Georgelin & Georgelin 1976; Imai et al. 2000). Therefore, the three fields fall in a ∼2000 AU diameter region. Figures 2, 3, and 4 show these masers in greater detail. The positions, peak flux densities (S_{max}), and the deconvolved angular sizes were obtained from Gaussian fits. In field 3, three Gaussian components were used, and these are labeled North, Center, and South (N, C and S). Data from the fits are shown in Table 4. The absolute accuracy of the positions is estimated to be ±1 mas while the accuracy of the relative positions within W3(OH) is ∼0.1 mas. Therefore, to within the estimated uncertainties in absolute positions (±1 mas and ±5 mas), the positions marginally agree with those determined by GCRYF.

The minor axes of the masers are in the range 1.2 – 5.2 mas (2.4 – 6.2 AU). In fields 2 and 3 the sources are elongated by factors of 3 – 5. Furthermore, inspection of Table 3 shows that the VLBA recovered only about 30% of the total 4765 MHz line flux from W3(OH). Figure 5 is a superposition of the VLA and VLBA spectra. From comparison of the spectra, it is clear that 1) all of the W3(OH) maser features are partially spatially resolved, 2) the V=-45 km s^{-1} feature (field 3) is heavily resolved because this feature is much less intense in the VLBA data, and 3) the "plateau" between the two maxima in the VLA spectra is completely resolved by the VLBA. Even allowing for the difference in velocity resolution, the spectra of all of the individual features observed with the VLBA are noticeably narrower in velocity that the corresponding features observed with the VLA.

From the VLA observations, the position of the "plateau" feature is: $\alpha(J2000) = 02\ 27\ 03.81$, $\delta(J2000) = 61\ 52\ 24.3$, very close to the position of the maser in field 2. (The uncertainty in this VLA position is estimated to be $\pm 0.2''$ because of blending in the VLA data with the stronger nearby features in fields 1 and 3). Therefore, we can exclude the possibility that the "plateau" was outside of our field of view with the VLBA. From the VLA observations, the size of the plateau feature is $<0.5''$ x $<0.2''$. Non-detection of the plateau in VLBA observations constrains its size to be ≥60 mas. The two sets of observations constrain the brightness temperature, T_b, of this feature:

$1.2\ 10^5\ \mathrm{K} \leq \mathrm{T}_b \leq 3.2\ 10^6\ \mathrm{K}$.

The polarization measurements yielded only upper limits. For each Stokes parameter, we integrated the flux density over the source in each field. The upper limits for Q, U, and V are expressed as a percentage of I in Table 5. From VLA observations, we an find that the upper limit for V integrated over all of the W3(OH) masers is: V $\leq$ 0.8% I (4 σ).

4.1.2. 1720 MHz Observations

The positions, peak flux densities, deconvolved angular sizes, and V_{LSR} of the peaks of the 1720 MHz features are presented in Table 6. The synthesized beam is 6.2 mas x 5.5 mas at a position angle of 49°. The values for both the left and right circularly polarized (LCP and RCP) features are listed for the same fields used to describe the 4765 MHz observations above. The LCP and RCP features appear to be Zeeman pairs because they have the same positions to within 2 mas. Table 7 is a comparison between the 1720 MHz and 4765 MHz results. In this table, the first two columns provide the separation of the 1720 MHz LCP feature(s) from the 4765 MHz feature; the third and fourth columns, the corresponding separations for the 1720 RCP feature(s); the fifth, the parallel component of the magnetic field ($\mathrm{B}_{\|}$) computed from the velocity splitting (Lo et al. 1975; Gray et al. 2001). The sixth column provides the "demagnetized velocity" – the velocity that the feature would have in the absence of Zeeman splitting. The last column provides δV, the difference between the demagnetized velocity of the 1720 MHz features and the velocity of the 4765 MHz features. The demagnetized velocity is used in this comparison because the 4765 MHz features have no Zeeman splitting. The offsets are given in the sense 1720-4765. The sign of $\mathrm{B}_{\|}$ is the same at all six positions in W3(OH); values are 5.4 – 10.0 mG.

In Field 1, the 1720 MHz features occur in three clumps. As a function of velocity, the peak position moves approximately along a northwest to southeast line, both within and between clumps. The same pattern was noticed by Masheder et al. (1994). The positions tabulated are the positions with maximum intensity within each of the three clumps. In Field 1, the nearest 1720 MHz feature is displaced >190 mas from the 4765 MHz position. Near the position of the 4765 MHz feature (see Figure 2 and Table 4), the upper limit for any 1720 MHz emission is 75 mJy (4σ). The first feature in Field 2 in Table 6 differs in position from the 4765 MHz feature by 5±5 mas and in velocity by -0.06±.08 km s^{-1}. The second feature differs from the 4765 MHz feature in position by ∼18±5 mas and its velocity differs by ∼0.6±.08 km s^{-1}. In Field 3, the only 1720 MHz feature is very elongated N-S, and differs in position with the 4765 MHz feature called Field 3N by ∼5±7 mas and in velocity by 0.04±.08 km s^{-1}. While Masheder et al. (1994) found that some of the 1720 MHz masers had sizes ≤1.2 mas, we find no features with sizes <∼2 mas. The sizes of the 1720 MHz features in this data are all ≥ 2.7 mas.

Our 1720 MHz positions and those found by GCRYF with a 130 mas synthesized beam are plotted in Figure 3 and Figure 4. In GCRYF's study, conducted with a 40 mas beam at 4765 MHz,

two of the 4765 MHz sources (Fields 2 and 3) showed spatial coincidence with 1720 MHz emission. This finding is supported and refined in our study with a factor of 10 smaller beam. In Fields 2 and 3, the positional differences are less than our estimated absolute positional accuracy, and the velocity differences are much less than our velocity resolution at 4765 MHz. Therefore, to within the accuracy of our absolute position determinations (∼5 mas), there are 1720 MHz masers at the same positions as 4765 MHz masers in Fields 2 and 3N. Nevertheless, there are no corresponding 1720 MHz masers for the 4765 MHz masers in Fields 1, 3C and 3S. In addition, four 1720 MHz Zeeman pairs have no corresponding 4765 MHz masers. Further details of the 1720 MHz observations will be reported separately.

4.2. K3-50

With the 4.4 mas x 3.9 mas beam, K3-50 is a single, slightly resolved source. The peak flux density is ∼0.6 Jy/beam. Both a comparison between the spectra measured with the VLBA and the VLA (Figure 5) and the integrated line flux (Table 3) show that the VLBA recovers all of the 4765 MHz line flux from this source. The absolute position of the maser is given in Table 4. The accuracy of this position is estimated to be ±1 mas (see Section 2). The emission in the channel with maximum intensity is shown in Figure 6. Unlike W3(OH), there is no known nearby 1720 MHz maser. The nearest 1720 MHz maser is ON-3, ∼2.3′ northeast of the 4765 MHz maser.

The accepted distance for K3-50 is 7.4 kpc (i.e. Harris (1975); scaled to 8.5 kpc distance to the Galactic center). Because of the greater distance, it is not surprising that this source is less resolved than either W3(OH) or DR21EX. However, like W3(OH), the source is resolved with a linear size of 6.3 mas x 2.8 mas (∼ 50 x 20 AU). The polarization upper limits are summarized in Table 5.

4.3. DR21EX

DR21EX has six distinct maser spots which lie along an arc with angular extent ∼0.25″. At the estimated distance (2 kpc: Dickel et al. (1978)), this extent corresponds to ∼500 AU. The synthesized beam is 5.7 x 4.4 mas at a position angle of 23°. As explained in Section 2, absolute positions cannot be obtained for this source due to the lack of a phase-referencing source. All positions were referenced to the strongest component (feature 2). Our best estimate for this position from VLA observations is: $\alpha(J2000)$ = 20 39 00.377±.008, $\delta(J2000)$ = 42 24 37.28±.07. The relative locations of the six spots are shown in Figure 7. The six spots are approximately along a N-S arc, and their velocities increase from North to South. The measured parameters for each spot are presented in Table 4. The positions (referenced to the VLA position of feature 2), peak flux densities, LSR velocities, and deconvolved sizes are summarized in Table 4. The degree of resolution varies significantly from feature to feature (see Figure 5). The minor axes of the spots

range from $\sim$4 – $\sim$8 AU, and they are typically elongated by less than a factor of two. Comparison of the flux measured with the VLA shows that the VLBA observation recovers about 60% of the total flux (see Table 3). Therefore, a significant component of 4765 MHz emission is not detected by the VLBA. As was true for W3(OH), the components detected with the VLBA have noticeably narrower velocity widths that those detected with the VLA.

In VLA B-array observations on 2000 January 30, several 1720 MHz OH maser features were found within $0.2''$ of the 4765 MHz masers in this source (P. Palmer & W. M. Goss, in preparation). However, improved angular resolution at 1720 MHz and phase-referencing for both frequencies are needed to determine if the 4765 MHz and 1720 MHz masers coincide. The results of the polarization measurements are provided in Table 5.

Table 4: 4765 MHz Maser Parameters from VLBA Observations

Source	Field	α_{J2000}	δ_{J2000}	S_{max} (mJy/bm)	V_{LSR} (km s^{-1})	Size (mas)
W3(OH)	1	02 27 03.8311	61 52 25.097	410	-43.28	2.6 x 0.9
W3(OH)	2	02 27 03.8120	61 52 24.140	42	-43.39	13 x 3.9
W3(OH)	3 N	02 27 03.7126	61 52 24.661	33	-45.0	20 x 3.9
W3(OH)	3 C	02 27 03.7118	61 52 24.642	32	-45.0	11 x 4.0
W3(OH)	3 S	02 27 03.7125	61 52 24.633	26	-45.0	15 x 5.5
K3-50		20 01 45.7249	33 32 44.938	620	-20.35	6.3 x 2.8
DR21EX	1	20 39 00.3801	42 24 37.332	540	2.37	5.2 x 2.9
DR21EX[a]	2	20 39 00.3770	42 24 37.280	890	3.48	4.7 x 3.2
DR21EX	3	20 39 00.3759	42 24 37.259	250	3.72	5.1 x 3.9
DR21EX	4	20 39 00.3772	42 24 37.204	380	4.46	6.2 x 1.8
DR21EX	5	20 39 00.3780	42 24 37.190	440	4.95	6.8 x 3.7
DR21EX	6	20 39 00.3791	42 24 37.111	320	5.69	4.1 x 3.1

[a]All DR21EX positions are referenced to the VLA determination of the position of this component (see text).

Table 5: Upper Limits for 4765 MHz Polarization

Source	Field	Q (% of I)	U (% of I)	V (% of I)
W3(OH)	1	$\leq$2	$\leq$2	$\leq$4
W3(OH)	2	$\leq$12	$\leq$12	$\leq$12
W3(OH)	3	$\leq$12	$\leq$12	$\leq$7
K3-50		$\leq$4	$\leq$4	$\leq$4
DR21EX	1	$\leq$5	$\leq$5	$\leq$5
DR21EX	2	$\leq$3	$\leq$3	$\leq$3
DR21EX	3	$\leq$11	$\leq$11	$\leq$11
DR21EX	4	$\leq$6	$\leq$6	$\leq$6
DR21EX	5	$\leq$6	$\leq$6	$\leq$6
DR21EX	6	$\leq$11	$\leq$11	$\leq$11

Table 6: 1720 MHz VLBA Observations of W3(OH)

α_{J2000}	δ_{J2000}	S_{max} (Jy/bm)	Size (mas)	V_{LSR} (km s^{-1})
LCP				
Field 1				
02 27 03.8364	61 52 25.317	9.1	2.9x2.5	-43.47
02 27 03.8336	61 52 25.305	0.15	4.0x1.9	-44.91
02 27 03.8324	61 52 25.295	20.8	3.7x2.4	-45.60
Field 2				
02 27 03.8116	61 52 24.144	2.9	7.2x3.6	-43.77
02 27 03.8101	61 52 24.153	0.21	7.1x5.2	-44.53
Field 3				
02 27 03.7121	61 52 24.664	0.15	35x7	-45.26
RCP				
Field 1				
02 27 03.8364	61 52 25.317	14.6	2.8x2.6	-42.70
02 27 03.8338	61 52 25.306	0.12	4.5x3.3	-43.98
02 27 03.8323	61 52 25.293	15.5	3.8x2.5	-44.87
Field 2				
02 27 03.8116	61 52 24.143	2.7	7.4x3.8	-43.13
02 27 03.8102	61 52 24.152	.88	6.4x4.3	-43.43
Field 3				
02 27 03.7120	61 52 24.663	0.13	31x8	-44.66

Table 7: Comparison of 4765 and 1720 MHz Positions and Velocities in W3(OH)

$\Delta\alpha$ (mas)	$\Delta\delta$ (mas)	$\Delta\alpha$ (mas)	$\Delta\delta$ (mas)	$B_{\|\|}$ (mG)	V_* (km s^{-1})	δV (km s^{-1})
LCP		RCP				
Field 1						
38	220	37.1	220	7.0	-43.08	0.20
18	208	20	209	8.4	-44.44	-1.63
9.5	198	8.3	196.4	6.6	-45.24	-1.96
Field 2						
-2.5	3.8	-3.0	3.3	5.8	-43.45	-0.06
-14	13	-12	12	10.0	-43.98	-0.59
Field 3[a]						
-3.7	3.2	-4.2	2.0	5.4	-44.96	+0.04

[a]Comparisons with 4765 MHz Field 3N

5. Discussion

We provide an overview of the observational results:

- Co-propagation of 4765 MHz and 1720 MHz emission:

  In W3(OH), the maser positions in Fields 2 and 3 are compatible with models that require coincidence between the masers in the two transitions. However, Field 1 shows no such coincidence. Therefore, it is clear that not all 1720 MHz masers have detectable 4765 MHz counterparts and not all 4765 MHz features have detectable 1720 MHz counterparts; however, in some cases 4765 MHz and 1720 MHz emission can arise from regions separated by <10 AU. Lockett et al. (1999) find that as population in the $^2\Pi_{1/2}, J = 1/2$ state increases in their models, the far-IR lines connecting this state to the ground $^2\Pi_{3/2}, J = 3/2$ state "turn off" the 1720 MHz maser. However, a detectable 4765 MHz line requires that the $^2\Pi_{1/2}, J = 1/2$ state is populated. Producing the two masers simultaneously seems likely only for a narrow range of conditions. Therefore, the observations are compatible with co-propagation models if these models allow widely varying intensity ratios of 4765 MHz to 1720 MHz emission in order to produce observable intensities in either of the masers or both.

- Angular Sizes:

  In both W3(OH) and DR21EX, a significant fraction of the flux was resolved out with the VLBA; nevertheless a number of features have minor axes ranging from ∼1 – 5 mas. Many of the features were elongated by ≥ 3:1. The picture that emerges is that OH 4765 MHz emission occurs in regions 100's of AU in diameter in these sources, and that 30 – 60% of the flux density is confined to sources with diameters of 10's of AU. Furthermore, typically emission occurs over a velocity range ∼4 km s^{-1}, however, emission from the individual small spots has narrow velocity widths (typically ≤0.2 km s^{-1}).

- Brightness Temperatures:

  Brightness temperatures for the 4765 MHz maser positions measured with the VLBA are summarized in Table 8. The 4765 MHz maser brightness is listed in the third column; the corresponding 1720 MHz brightness in the fourth. The brightness temperatures at 4765 MHz range from 2 x 10^7 K to 5 x 10^9 K. Assuming that the fraction of flux density not detected with the VLA arises from sources >60 mas, the upper limit for the brightness temperatures of the diffuse components is $T_b \leq 3\ 10^6$ K (see section 4.1.1). The 1720 MHz brightness exceeds that at 4765 MHz by factors of 10 – 1000.

The above summary may be used to place constraints on the physical conditions in the regions of maser emission.

Table 8: Source Brightness Temperatures at 4765 MHz Maser Positions

Source	Field	T_b(4765) (K)	T_b(1720) (K)
W3(OH)	1	$5\ 10^9$	
W3(OH)	2	$4\ 10^7$	$4\ 10^{10}$
W3(OH)	3 N	$2\ 10^7$	$2\ 10^8$
W3(OH)	3 C	$4\ 10^7$	
W3(OH)	3 S	$2\ 10^7$	
K3-50		$2\ 10^9$	
DR21EX	1	$2\ 10^9$	
DR21EX	2	$3\ 10^9$	
DR21EX	3	$6\ 10^8$	
DR21EX	4	$2\ 10^9$	
DR21EX	5	$9\ 10^8$	
DR21EX	6	$1\ 10^9$	

(1) The state of saturation of the masers: the rate of depopulation of the upper level by stimulated emission is $W_{stim} = A_{ul}\frac{kT_b}{h\nu}\frac{\Omega_M}{4\pi}$, where Ω_M is the solid angle from which a typical molecule in the source receives radiation at brightness temperature T_b. For the 4765 MHz line, A_{ul} = 3.89 10^{-10} s^{-1} (Destombes et al. 1977), and we take $\frac{\Omega_M}{4\pi}$ ∼1/2 to obtain $W_{stim} = 9\ 10^{-9} T_b$ s^{-1}. We estimate the collisional rate as $W_{col} \sim 10^{-10} n_{H_2}$ s^{-1}. Therefore, if $T_b \sim 10^{10}$ K, W_{stim} will exceed other rates as long as $n_{H_2} \leq 9\ 10^{11}$ cm^{-3}. (All OH pumping models to date assume densities $\ll 10^{11}$ cm^{-3}). Therefore, this brightness temperature implies that the maser is saturated unless the emission region is significantly elongated along the line of sight so that the value of Ω_M is seriously overestimated above. However, for the surrounding regions with lower brightness, the density upper limit to avoid saturation is $n_{H_2} \leq 3\ 10^7$ cm^{-3}. Thus, the high brightness temperature spots are almost certainly saturated, although the more extended 4765 MHz emission may not be. It has frequently been assumed that rapid time-variations are an indicator of an unsaturated maser (e.g. Persi et al. (1994); Caswell et al. (1995); Desmurs & Baudry (1998)). If this assumption is correct for the 4765 MHz masers reported in this paper, the conclusion from the above consideration of the saturation state of the maser is in conflict with the observational data for 4765 MHz masers.

(2) We examine the maser optical depth required to produce a brightness T_b: the line center optical depth is:

$$\tau_0 = \sqrt{\frac{4ln(2)}{\pi}}\frac{c^2}{8\pi\nu^2}\frac{A_{ul}}{g_u\Delta\nu}\Delta n L, \tag{1}$$

where Δn is the population difference (per magnetic sub-level) of the upper (u) and lower (l) energy levels involved in the transition, and L is the pathlength. That is,

$$\Delta n = \frac{n_l}{g_l} - \frac{n_u}{g_u}. \tag{2}$$

Inserting appropriate constants for this transition and $\Delta\nu$=3 kHz (∼0.2 km s^{-1}, corresponding to the narrow lines observed with the VLBA), equation(1) becomes:

$$\tau_0 = 6.4\ 10^{-14}\Delta n\ L. \tag{3}$$

To express Δn in terms of the total density of molecular gas, we write:

$$\Delta n = -\tfrac{1}{2}\eta y f n_{H_2}. \tag{4}$$

Here, η is the inversion efficiency ($\frac{n_u - n_l}{n_u + n_l}$; Lockett et al. 1999), y is the fraction of OH molecules in the $^2\Pi_{1/2}, J = 1/2$ state, f is the fractional abundance of OH compared to H_2, and the factor 1/2 is present because the population of the state is approximately equally distributed among the sub-levels of the four hyperfine levels at plausible temperatures and inversion fractions.

We express the pathlength in AU, and obtain:

$$\mid \tau_0 \mid = 0.48\ y\eta f n_{H_2} L_{AU}. \tag{5}$$

For temperatures between 50 – 200 K, y is in the range 0.03 – 0.1, and η is estimated to lie in the range 0.01 – 0.1. Taking the geometric mean of possible values of the product, $y\eta = 1.3\ 10^{-3}$, we obtain:

$$\mid \tau_0 \mid = 8\ 10^{-4}\ f n_{H_2} L_{AU}. \tag{6}$$

For an OH abundance fraction f$\sim 10^{-5}$ (see Pavlakis & Kylafis 1996a and references therein), we obtain:

$$\mid \tau_0 \mid = 8\ 10^{-9}\ n_{H_2} L_{AU}. \tag{7}$$

There is little doubt that the product $y\eta$ has an uncertainty of less than an order of magnitude. While f is at the upper end of possible values for relative abundance of OH to H_2 in the interstellar medium (i.e. within a factor of a few of the total O abundance), all models for OH masers to date have invoked an increased OH fractional abundance.

The brightness temperature of the background is ≤ 10 K for the 4765 MHz masers reported in this paper. Therefore, in order to produce $T_b \sim 5\ 10^9$ K, a minimum gain corresponding to $\mid \tau_0 \mid \sim 20$ is required. While the brightness temperatures are typically a factor of 10 less than is typical for OH masers (Elitzur 1992), these values of T_b still lead to rather severe constraints on parameters of the region. From equation (7) we find:

$$L_{AU} = \frac{2\ 10^9}{n_{H_2}}.$$

Therefore if L_{AU} is to be less than the diameter of the entire 4765 MHz maser region (taken to be 10^3 AU) we require $n_{H_2} \geq 2\ 10^6$ cm^{-3}. On the other hand, if the pathlength were comparable to the spot sizes ($\sim$10 AU), required densities would be increased by a factor of $\sim$100. We regard such a density as implausible (see also next paragraph). The density required can be reduced by a factor of 10 if the product $y\eta$ were taken to be at the extreme high end of the plausible range; however, the density would be increased by a factor of 10 if the product were at the low end. (The required density would be increased by another factor of 10 if the OH abundance were similar to that found in quiescent, low density regions of molecular clouds.)

The small measured transverse extent of each feature together with the $\sim$100 times greater pathlength along the line of sight inferred from limits on the density leads to the conclusion that the maser region is filamentary with the long direction pointed toward the observer. Such a structure also relieves the constraint on saturation derived above since Ω_M would be greatly reduced. These filaments need not be geometric structures, but may simply be lines of sight through the much larger region in which the velocity coherence is greatest. Such an interpretation fits naturally with the very narrow line widths detected with the VLBA. Where velocity coherence does not exist, lower brightness emission may be produced.

While many models for OH masers have been developed in the last 30 years, parity assignments for Λ-doublet levels of OH were incorrect until 1984, and collision cross sections before 1994 were significantly discrepant compared with the best current values (Pavlakis & Kylafis 1996a). Therefore, we primarily consider models developed since 1994.

First, we compare the density limit derived above for the 4765 MHz maser region with that derived from consideration of the 1720 MHz line. Lockett et al. (1999) find that the 1720 MHz maser is quenched by collisions at densities above $\sim 5\ 10^5 \mathrm{cm}^{-3}$. Therefore the density estimate derived above ($10^{6\pm1}$ cm^{-3}) can be compatible with 1720 MHz emission arising in the same physical region as 4765 MHz emission only if the density is near its lower limit. Pavlakis & Kylafis (1996a,b) have explicitly discussed the production of the 4765 MHz line and find no range of conditions in which simultaneous production of 4765 MHz and 1720 MHz masers can occur. In an earlier detailed model, Gray et al. (1992) can obtain coincidence of the 4765 MHz and 1720 MHz region with a density $2\ 10^7$ cm^{-3} in an accelerating flow. Apparently, radiative pumping in the flow is sufficient to overcome quenching; then the accelerating flow prevents the optical depth in the far IR lines connecting the $^2\Pi_{3/2}, J = 3/2$ and $^2\Pi_{1/2}, J = 1/2$ states from becoming large enough to quench the 1720 MHz maser. Because of the difficulty other models encounter finding physical conditions in which 1720 MHz and 4765 MHz emission both arise, further work on this model is desirable to verify if the results are qualitatively similar based on more recent collision cross sections.

A model using these recent collision cross sections was developed for 1720 MHz emission near supernova remnants (Lockett et al. 1999). This model also explains the enhanced OH abundance in a natural way. In this model, OH is formed behind a C-shock surrounding the supernova remnant. However, 4765 MHz emission is not explicitly discussed. In regions in which 4765 MHz emission is detected, there are certainly shocks caused by molecular outflows. However, these shocks are expected to be J-shocks. If a transverse magnetic field is present, an initial J-shock evolves into a C-shock (see e.g. Flower et al. 2003). The 5 – 10 mG magnetic fields found in the 1720 MHz observations are suggestive of C-shocks (see Table 7).

A requirement for future progress is the development of models for the 4765 MHz masers similar to the Lockett et al. (1999) models for 1720 MHz masers. These new models must use the improved collision cross sections and treat the transfer of the infrared lines which connect 1720 MHz and 4765 MHz lines.

In W3(OH) we confirmed with higher positional accuracy (≤ 5 mas) the agreement between the 4765 MHz and 1720 MHz maser positions. We also showed that to within VLA accuracy ($\sim 0.2''$), there are 1720 MHz masers in the region of 4765 MHz emission in DR21EX. There are no known 1720 MHz features in the Field 1 of W3(OH) and the K3-50 sources. We also detected no polarization for any of the 4765 MHz features. Upper limits in the best cases are $\sim 3\%$ (4σ).

VLA observations of K3-50 at 1720 MHz should be done to confirm the absence of a 1720 MHz maser at that location. Also, it is important to determine absolute positions for both 4765 MHz emission and 1720 MHz emission from DR21EX.

K. Devine would like to thank the NRAO and the NSF for making this research experience possible and C. Brogan and E. Greisen for their assistance throughout the summer. P. Palmer thanks the NRAO for hospitality during several extensive visits while this work was carried out.

REFERENCES

Baudry, A., Diamond, P. J., Booth, R.S., Graham, D., & Walmsley, C. M. 1988, A&A, 201, 105

Caswell, J. L., Vaile, R. A., Ellingsen, S. P., & Norris, R. P. 1995, MNRAS, 274, 1126

Cesaroni, R. & Walmsley, C. M. 1991, A&A, 241, 537

Cohen, R. J., Masheder, M. R. W., Caswell, J. L. 1995, MNRAS, 274, 808

Cohen, R. J., Masheder, M. R. W., Walker, R. N. F. 1991, MNRAS, 250, 611

Desmurs, J. F., & Baudry, A. 1998, A&A, 340, 521

Destombes, J. L., Marliere, C., Baudry, A., & Brillet, J. A&A, 60, 55

Dickel, J. R., Dickel, H. R., Wilson, W. J. 1978, ApJ, 223, 840

Dodson, R. G., Ellingsen, S. P. 2002, MNRAS, 333, 307

Dousmanis, G. C., Sanders, Jr., T. M., & Townes, C. H. 1955, Phys. Rev., 100, 1735

Elitzur, M. 1992, Astrophysical Masers (Dordrect: Kulwer).

Flower, D. R., Le Bourlot, J., Pineau des Fortês, & Cabrit, S. 2003, MNRAS, 341, 70

Gardner, F. F., Whiteoak, J. B., Palmer, P. 1983, MNRAS, 205, 297

Georgelin, Y. M., & Georgelin, Y. P. 1976, A&A, 49, 57

Gray, M. D., Field, D., & Doel, R. C. 1992, ApJ, 350, 209

Gray, M. D., Cohen, R. J., Richards, A. M. S, Yates, J. A., & Field, D. 2001, MNRAS, 324, 643 (GCRYF)

Harris, S. 1975, MNRAS, 170, 139

Imai, H., Kameya, O., & Sasao, T. 2000, ApJ, 538, 751

Kylafis, N. D., & Norman, C. A. 1990, ApJ, 350, 209

Lo, K. Y., Walker, R. C., Burke, B. F., Moran, J. M., Johnston, K. J., & Ewing, M. S. 1975, ApJ, 202, 650

Lockett, P., Gauthier, E., & Elitzur M. 1999, ApJ 511,235

Masheder, M. R. W., Field, D., Gray, M. D., Migenes, V., Cohen, R. J., & Booth, R. S. 1994 A&A, 281, 871

Palmer, P., Whiteoak, J. B., & Goss, W. M. 2003, MNRAS, submitted

Pavlakis, K. G., & Kylafis, N. D. 1996a, ApJ, 467, 300

Pavlakis, K. G., & Kylafis, N. D. 1996b, ApJ, 467, 309

Persi, P., Palagi, F., & Felli, M. 1994, A&A, 291, 983

Smits, D. P. 1997, MNRAS, 287, 253

Smits, D. P., Cohen, R. J., Hutawarakorn, B. 1998, MNRAS, 296, L11

Zuckerman, B., Palmer, P., Penfield, H, Lilley, A. E. 1968, ApJ, 153, L69

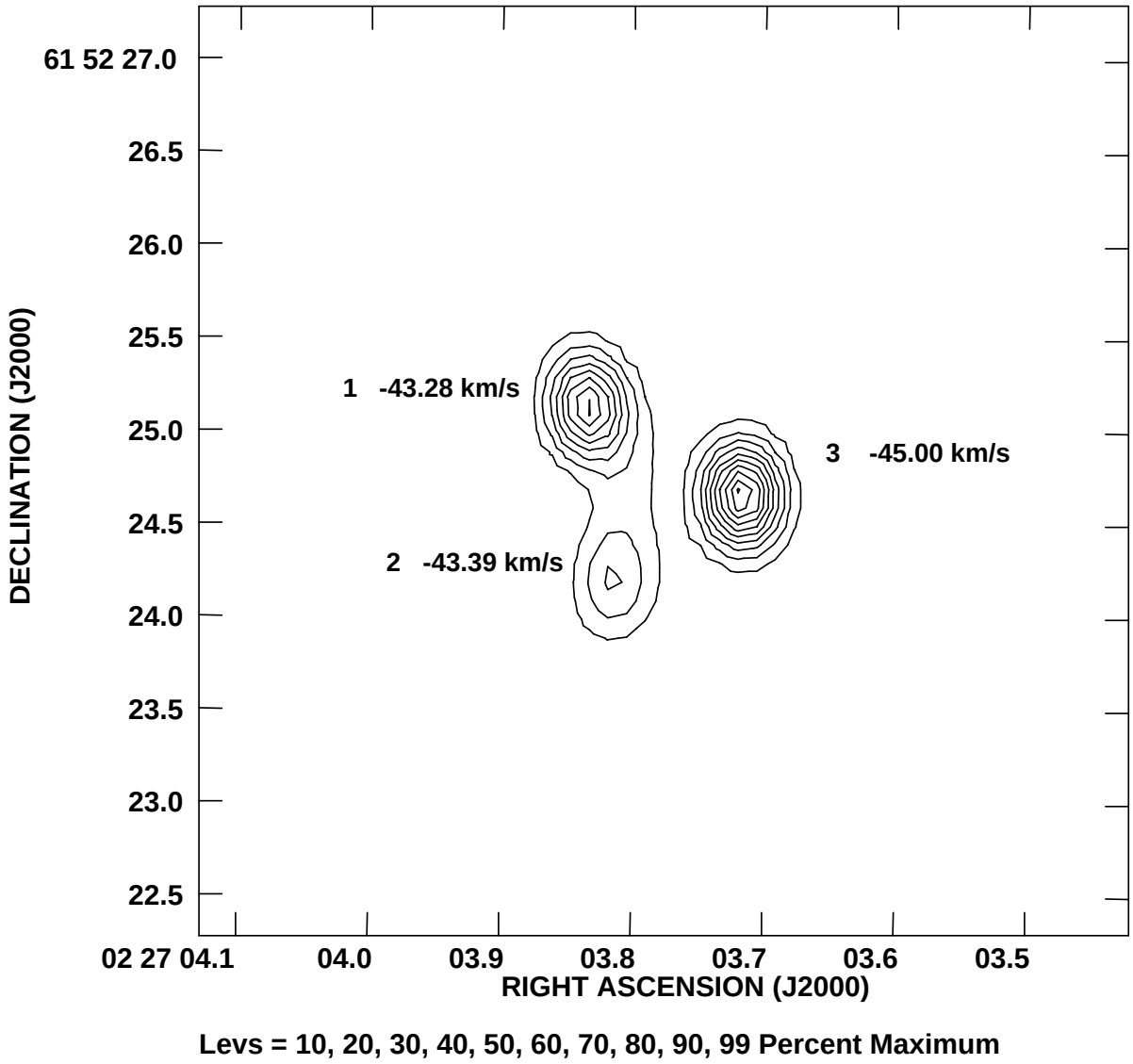

Fig. 1.— W3(OH) integrated line emission observed with the VLA (beam: 0.4″ x 0.3″, PA= 6°). The contours show $\int S(v)dv$ relative to the largest value (feature 3). The number used to identify the field and the V_{LSR} of the maximum in that field are shown. Fields 1, 2, and 3 imaged with the VLBA (Figures 2, 3, and 4) correspond to the three peaks in this VLA image.

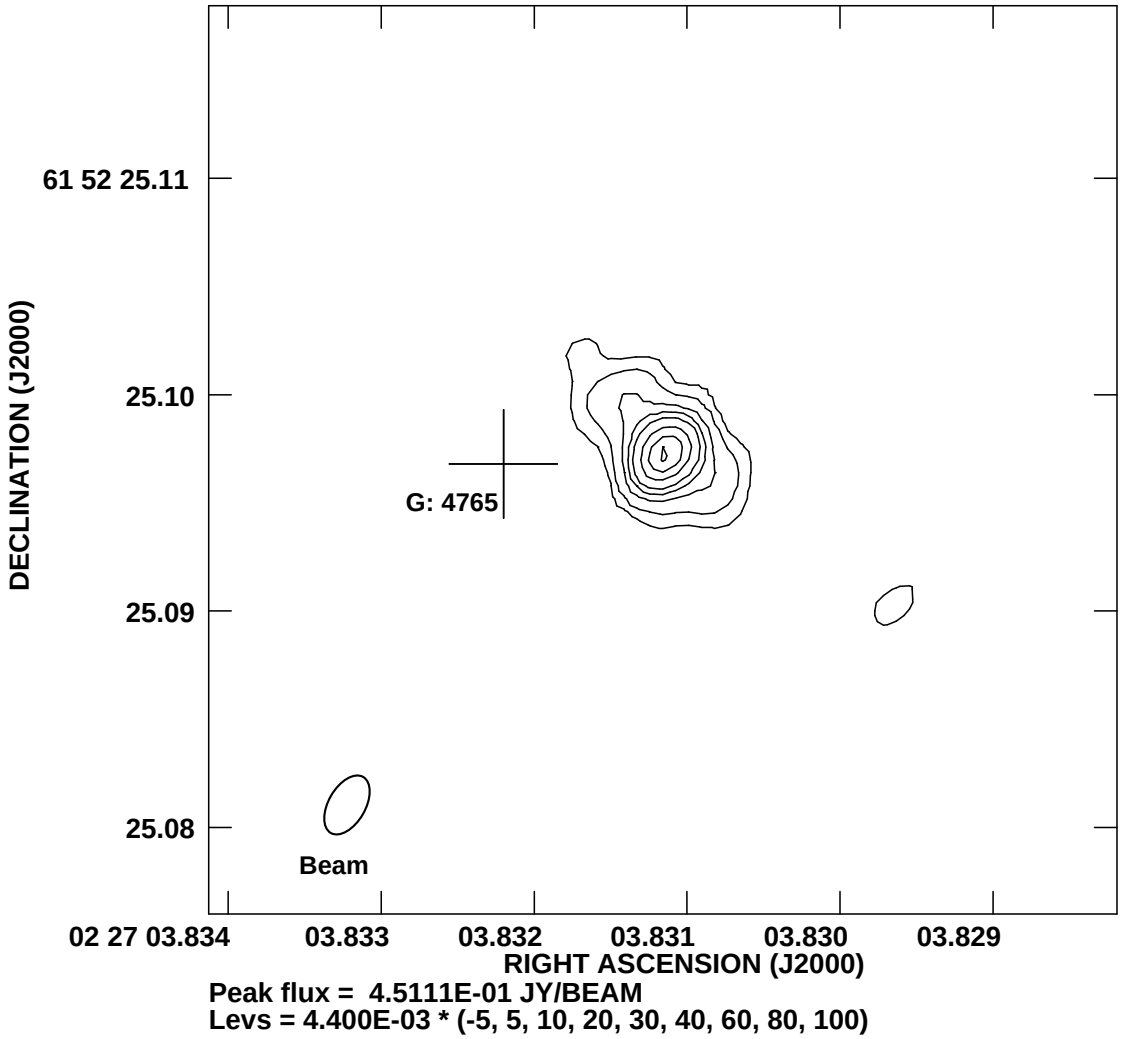

Fig. 2.— The contours indicate the 4765 MHz emission from Field 1 of W3(OH) in the channel with maximum intensity (V_{LSR}= -43.38 km s^{-1}). The position found by GCRYF for 4765 MHz emission is indicated. The offset between the GCRYF position and the position determined in this paper is 8 mas. The estimated absolute positions errors are ±5 mas for GCRYF and ±1 mas for this paper. Therefore the offset is marginally significant. The nearest 1720 MHz features are $\sim 0.2''$ north. Contours are in units of the RMS noise (4.4 mJy). The synthesized beam (2.9 mas x 1.6 mas) is shown in the lower left corner.

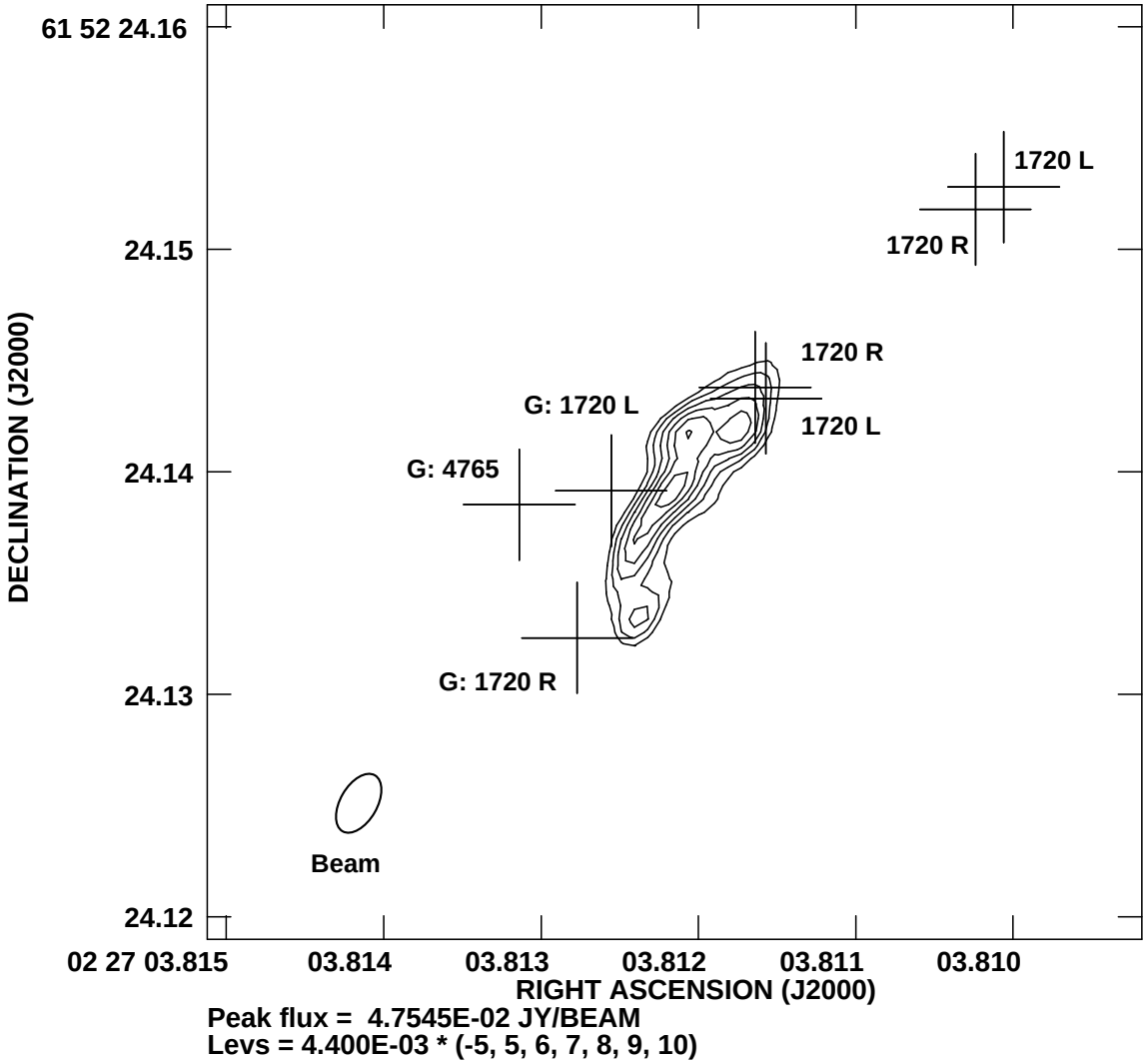

Fig. 3.— The contours indicate the 4765 MHz emission from Field 2 of W3(OH) in the channel with maximum intensity (V_{LSR}= -43.52 km s^{-1}). The 1720 MHz positions are indicated by crosses. The GCRYF positions for 4765 MHz and 1720 MHz emission are also indicated (prefixed by G:). At 1720 MHz, the estimated absolute positions errors are ±15 mas for GCRYF and ±5 mas for this paper. Therefore the offset between the two determinations of 1720 MHz positions is not significant. The offset between the two 4765 MHz positions is 8 mas. At 4765 MHz, the estimated absolute positions errors are ±5 mas for GCRYF and ±1 mas for this paper. Therefore the offset at 4765 MHz is marginally significant. Contour scheme and synthesized beam: as in Figure 2.

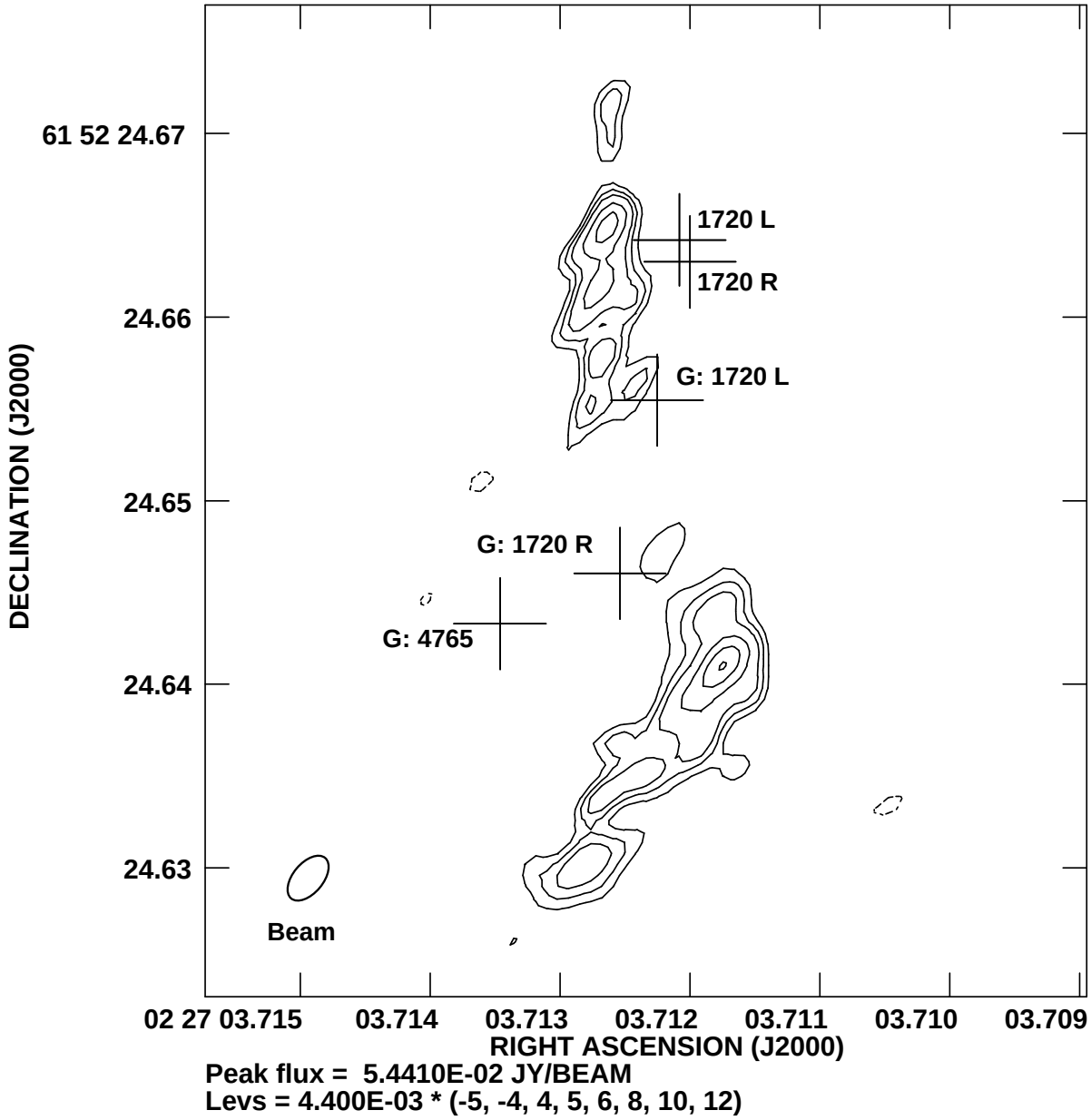

Fig. 4.— The contours indicate the 4765 MHz emission from Field 3 of W3(OH) in the channel with maximum intensity (V_{LSR}= -45.00 km s^{-1}). The 1720 MHz positions are indicated by crosses. The GCRYF positions for 4765 MHz and 1720 MHz emission are indicated (prefixed by G:). Note that with the increased angular resolution of our observations, the source is heavily resolved and at least two maxima are evident. The 1720 MHz emission, although elongated N-S, does not extend to the location of the southern 4765 MHz complex. Because of the absolute position errors in GCRYF and this paper as well as the complex source distribution at the current resolution, the offsets between GCRYF and this paper are not significant. Contour scheme and synthesized beam: as in Figure 2.

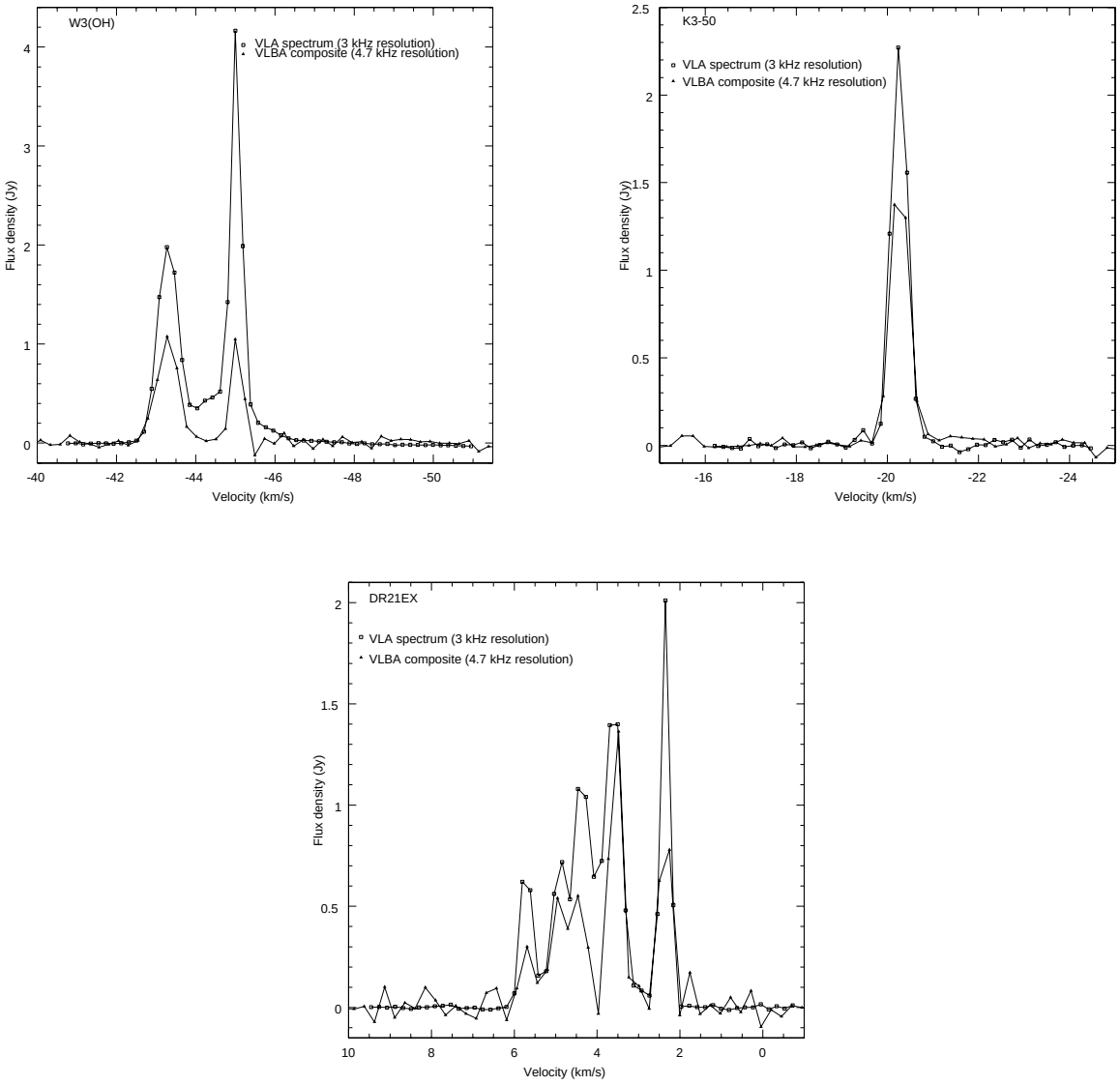

Fig. 5.— Comparison of VLA and VLBA spectra for W3(OH), K3-50, and DR21EX. Note that the velocity resolutions are slightly different, so that very narrow features are expected to have somewhat lower peak flux densities in VLBA than in VLA spectra. The integral over the spectrum is unaffected. See Tables 2 and 3 for observational details.

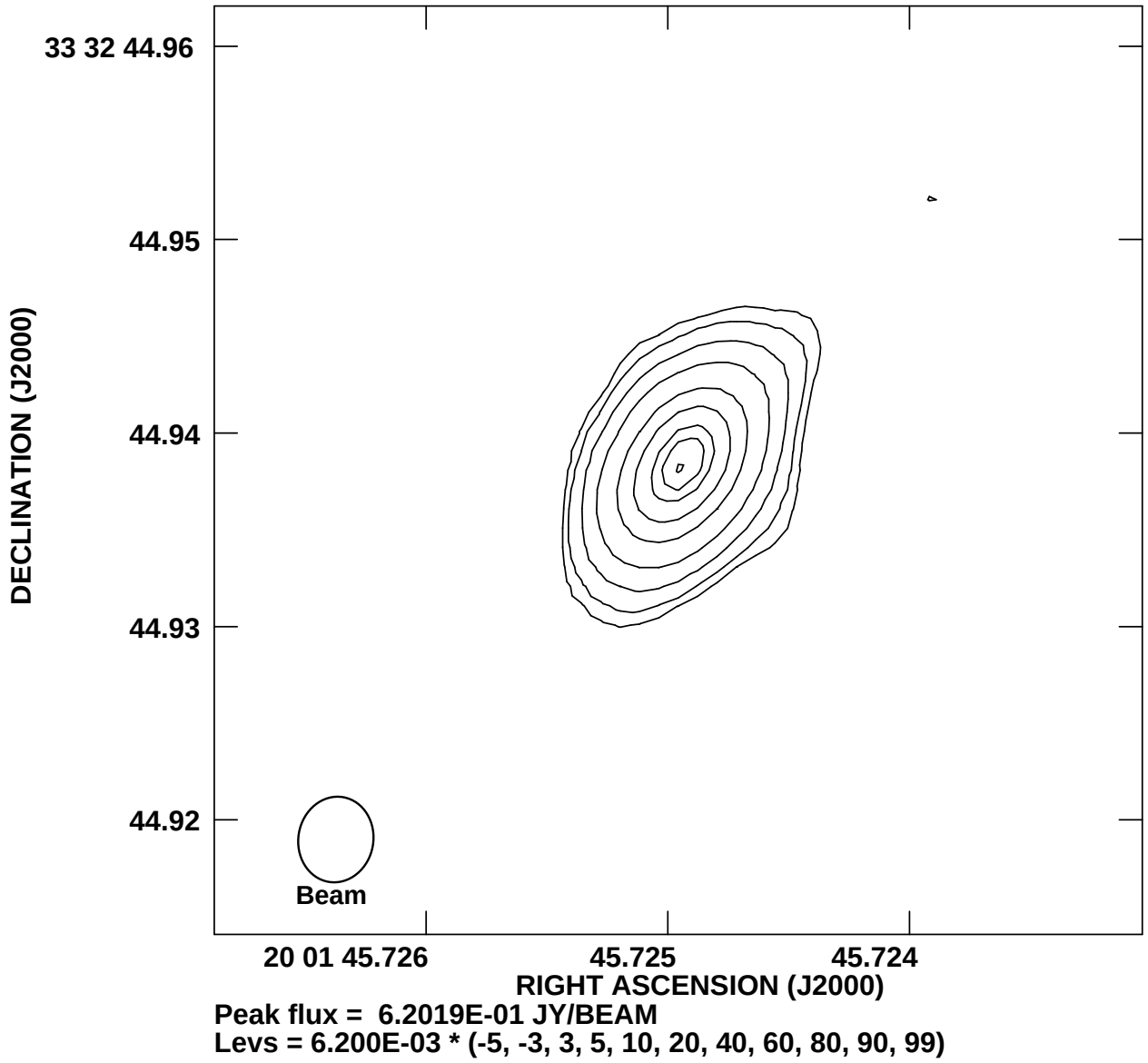

Fig. 6.— The contours indicate the 4765 MHz emission brightness in the channel with maximum intensity (V_{LSR}= -20.15 km s^{-1}) toward K3-50. Contours are in units of the RMS noise (6.3 mJy); the synthesized beam (4.4 mas x 3.9 mas) is shown in the lower left corner.

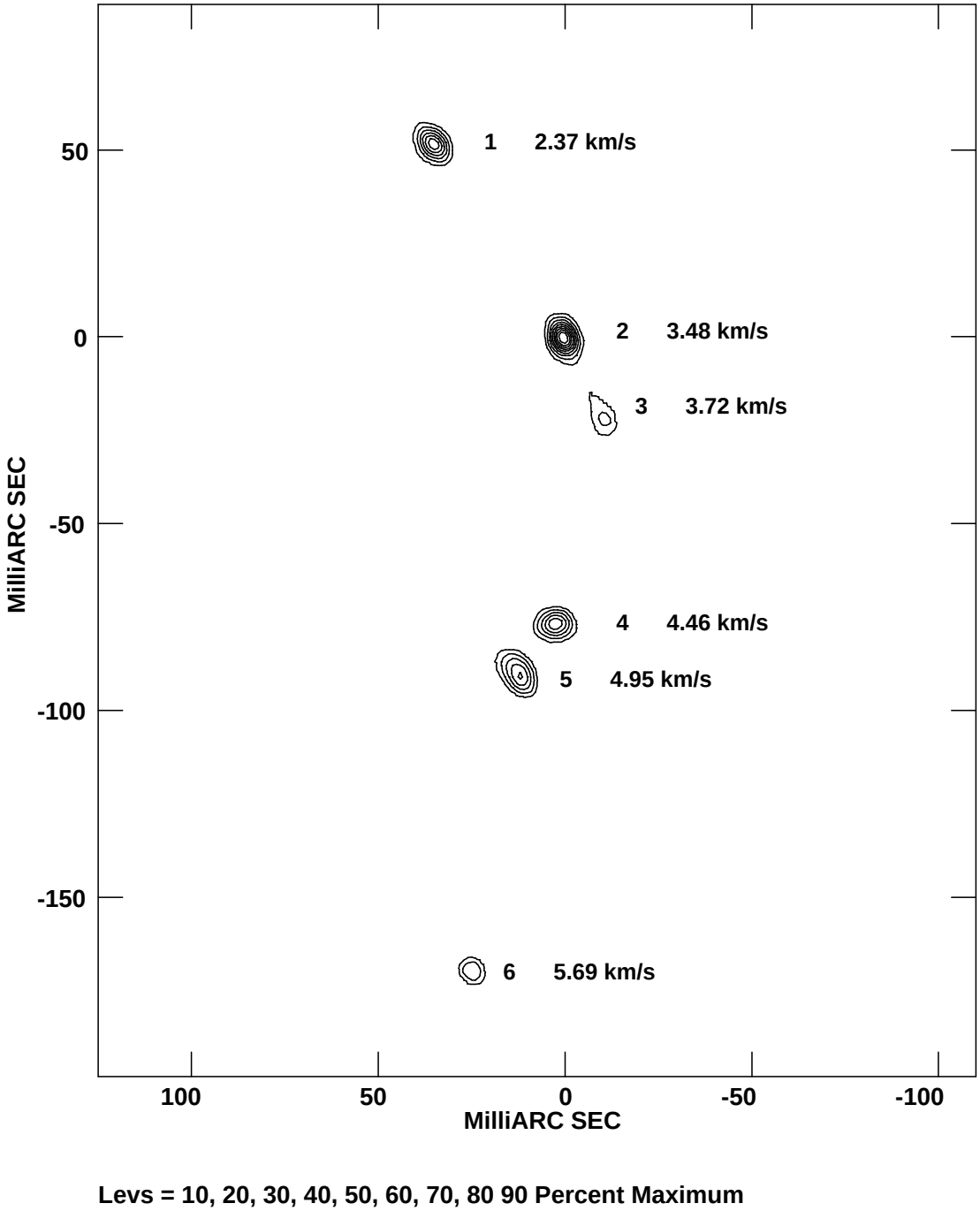

Fig. 7.— The contours indicate positions and integrated intensities ($\int S(v)dv$) of the six maser spots in DR21EX relative to the position and integrated intensity of feature 2. The number used to identify the feature and its V_{LSR} are shown. While the absolute positions of the features are not determined in the VLBA observation, the error in relative positions is $\leq$.1 mas. The synthesized beam is 5.7 mas x 4.4 mas, P.A.= 23°.